

Gradient Magnitude Similarity Deviation: A Highly Efficient Perceptual Image Quality Index

Wufeng Xue^a, Lei Zhang^b, *Member, IEEE*, Xuanqin Mou^a, *Member, IEEE*, Alan C. Bovik^c, *Fellow, IEEE*

^a Institute of Image Processing and Pattern Recognition, Xi'an Jiaotong University, Xi'an, China

^b Dept. of Computing, The Hong Kong Polytechnic University, Hong Kong, China

^c Dept. of Electrical and Computer Engineering, The University of Texas at Austin, Austin, TX, US

Abstract – Faithfully evaluating perceptual image quality is an important task in applications such as image compression, image restoration and multimedia streaming. A good image quality assessment (IQA) model is expected to be not only effective (i.e., deliver high quality prediction accuracy) but also computationally efficient. Owing to the need to deploy image quality measurement tools in high-speed networks, the efficiency of an IQA metric is particularly important due to the increasing proliferation of high-volume visual data. Here we develop and explain a new effective and efficient IQA model, called gradient magnitude similarity deviation (GMSD). Although the image gradient has been employed in other IQA models, few have achieved favorable performance in terms of both accuracy and efficiency. The results are proactive: we find that the pixel-wise gradient magnitude similarity (GMS) between the reference and distorted images combined with a novel pooling strategy – the standard deviation of the GMS map – predict accurately perceptual image quality. The resulting GMSD algorithm is much faster than most state-of-the-art IQA methods, and delivers highly competitive prediction accuracy on benchmark IQA databases. Matlab code that implements GMSD can be downloaded at <http://www4.comp.polyu.edu.hk/~cslzhang/IQA/GMSD/GMSD.htm>.

Index Terms – Gradient magnitude similarity, image quality assessment, standard deviation pooling, full reference

I. INTRODUCTION

In many image processing tasks (e.g., image acquisition, compression, restoration, transmission, etc.), it is necessary to evaluate the quality of the output image. Since human subjects are the ultimate observers and judges of image quality, it is highly desired to develop automatic approaches that can predict perceptual image quality consistently with human subjective evaluation. The traditional mean square error (MSE) or peak signal to noise ratio (PSNR) correlates poorly with human perception, and hence researchers have been devoting much effort in the development of advanced perception-driven image quality assessment (IQA) models [2, 25]. IQA models can be classified [3] into full reference (FR) ones, where the pristine reference image is available, no reference (NR) ones, where the reference image is not available, and reduced reference (RR) ones, where partial information of the reference image is available.

Here we focus on the area of FR-IQA models, which are widely used to evaluate a variety of image processing methods by measuring the quality of their output images. A good FR-IQA model can shape many image processing algorithms, as well as their implementation and optimization [1]. Generally speaking, there are two strategies for FR-IQA design. The first strategy follows a bottom-up framework [3, 30], which simulates the different processing stages in the visual pathway of human visual system (HVS), including the visual masking effect [32], contrast sensitivity [33], just noticeable differences [34], etc. However, the HVS is too complex and our current knowledge of it is still far from enough to construct an accurate bottom-up IQA framework to evaluate natural image quality. The second strategy adopts a top-down framework [3, 30, 4-8], which aims to model the overall function of the HVS based on some global assumptions on it. Many FR-IQA models follow this framework. The well-known Structure SIMilarity (SSIM) index [8] and its variants Multi-Scale SSIM (MS-SSIM) [17] and Information Weighted SSIM (IW-SSIM) [16] assume that the HVS tends to perceive the local structure in an image when evaluating its quality. The Visual Information Fidelity (VIF) [23] and Information Fidelity Criteria (IFC) [22] treat HVS as a communication channel and they predict the subjective image quality by computing how much the information within the perceived reference image is preserved in the perceived distorted one. Other state-of-the-art FR-IQA models that follow the top-down framework include the early vision based Ratio of Non-shift Edges (rNSE) [18, 24], phase congruency and gradient based Feature SIMilarity (FSIM) [7], etc. A comprehensive survey and comparison of state-of-the-art

IQA models can be found in [30, 14].

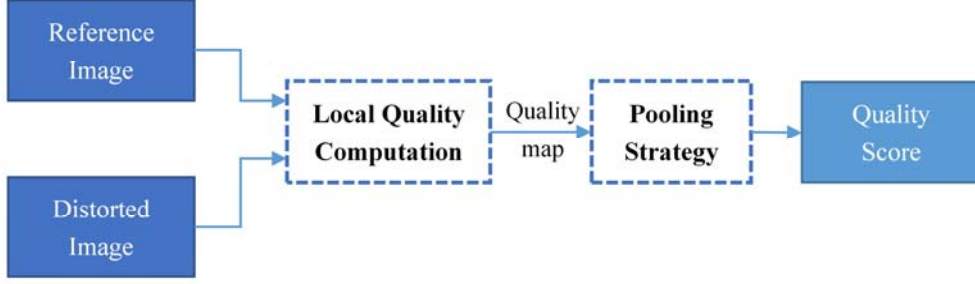


Figure 1: The flowchart of a class of two-step FR-IQA models.

Aside from the two different strategies used for FR-IQA model design, many IQA models share a common two-step framework [16, 4-8], as illustrated in Fig. 1. First, a *local quality map* (LQM) is computed by locally comparing the distorted image with the reference image via some similarity function. Then a single overall quality score is computed from the LQM via some *pooling* strategy. The simplest and widely used pooling strategy is average pooling, i.e., taking the average of all elements in LQM as the overall quality prediction. Since different regions may contribute differently to the overall perception of an image’s quality, the local quality values can be weighted to produce the final quality score. Example weighting strategies include local measures of information content [9, 16], content-based partitioning [19], assumed visual fixation [20], visual attention [10] and distortion based weighting [9, 10, 29]. Compared with average pooling, weighted pooling can improve the IQA accuracy to some extent; however, it may be costly to compute the weights. Moreover, weighted pooling complicates the pooling process and can make the predicted quality score be more nonlinear w.r.t. the subjective quality score (as shown in Table IV and Fig. 5), whereas linearity w.r.t. the subjective score is a desirable property of IQA algorithms. More discussions on linearity will be given in Section III-E.

In practice, an IQA model should be not only effective (i.e., having high quality prediction accuracy) but also efficient (i.e., having low computational complexity). With the increasing ubiquity of digital imaging and communication technologies in our daily life, there is an increasing vast amount of visual data to be evaluated. Therefore, efficiency has become a critical aspect of IQA algorithm. Unfortunately, effectiveness and efficiency are often hard to achieve simultaneously, and most previous IQA algorithms reach only one of the two goals. Towards contributing to filling this need, in this paper we develop an efficient FR-IQA model,

called gradient magnitude similarity deviation (GMSD), which computes the LQM by comparing the gradient magnitude maps of the reference and distorted images, and which uses the standard deviation of the LQM as the pooling strategy. The proposed GMSD is much faster than most state-of-the-art FR-IQA methods, but supplies surprisingly competitive quality prediction performance.

Using the image gradient to design IQA models is not new. The image gradient is a popular feature in IQA [4-7, 15, 19] since it can effectively capture image local structures, to which the HVS is highly sensitive. The most commonly encountered image distortions, including noise corruption, compression artifacts and image blur, will lead to highly visible structural changes that “pop out” of the gradient domain. Most gradient based FR-IQA models [5-7, 15] were inspired by SSIM [8]. They first compute the similarity between the gradients of reference image and distorted image, and then compute some additional information, such as the difference of gradient orientation, luminance similarity and phase congruency similarity, to combine with the gradient similarity for pooling. However, the computation of such additional information can be expensive and often yields small performance improvement.

Without using any additional information, we find that using the image gradient magnitude alone can still yield highly accurate quality prediction. The image gradient magnitude is responsive to artifacts introduced by compression, blurring or additive noise, etc. (please refer to Fig. 2 for examples). In the proposed GMSD model, the pixel-wise similarity between the gradient magnitude maps of the reference and distorted images is computed to create a LQM of the distorted image. Considering that natural images usually have many different local structures, and that different structures suffer different degradations in gradient magnitude, we compute the standard deviation of the gradient magnitude similarity induced LQM to generate the overall image quality score. The proposed standard deviation pooling based GMSD model leads to better accuracy than all state-of-the-art IQA metrics we can find, and it is very efficient, making large scale real time IQA possible. In addition, the proposed GMSD model has high linearity w.r.t. human subjective scores even without nonlinear regression.

The rest of the paper is organized as follows. Section II presents the development of GMSD in detail. Section III presents extensive experimental results, discussions and computational complexity analysis of the proposed GMSD model. Finally, Section IV concludes the paper.

II. GRADIENT MAGNITUDE SIMILARITY DEVIATION

A. Gradient Magnitude Similarity

The image gradient has been employed for FR-IQA in different ways [3, 4, 5, 6, 7, 15]. Most gradient based FR-IQA methods adopt a similarity function similar to that in SSIM [8] to compute gradient similarity. In SSIM, three kinds of similarities are computed, luminance similarity (LS), contrast similarity (CS) and structural similarity (SS), and the product of them is used to predict the image local quality at a position. Inspired by SSIM, Chen *et al.* proposed gradient SSIM (G-SSIM) [6]. They retained the LS term of SSIM but applied the CS and SS similarities to the gradient magnitude maps, denoted by \mathbf{m}_r and \mathbf{m}_d , of reference image \mathbf{r} and distorted image \mathbf{d} . As in SSIM, average pooling is used in G-SSIM to yield the final single quality score. Cheng *et al.* [5] proposed a geometric structure distortion (GSD) metric to predict image quality, which computes the similarity between the gradient magnitude, the gradient orientation (cosine of the angle difference) and contrast of \mathbf{r} and \mathbf{d} . Average pooling is also used in GSD. Liu *et al.* [15] also followed the framework of SSIM. They predicted the image quality using a weighted summation (i.e., a weighted average pooling strategy is used) of the squared luminance difference and the gradient similarity. Zhang *et al.* [7] combined the similarities of phase congruency and gradient magnitude between \mathbf{r} and \mathbf{d} . A phase congruency weighted average pooling method is used to produce the final quality score. The resulting Feature SIMilarity (FSIM) model is among the leading FR-IQA models in term of prediction accuracy. However, the computation of phase congruency features is very costly.

For digital images, the gradient magnitude is defined as the root mean square of image directional gradients along two orthogonal directions. The gradient is usually computed by convolving an image with a linear filter such as the classic Roberts, Sobel, Scharr and Prewitt filters and some task-specific ones [26, 27, 28]. For simplicity of computation and to introduce a modicum of noise-insensitivity, we utilize the Prewitt filter to calculate the gradient because it is the simplest one among the 3×3 template gradient filters. Other filters such as Sobel and Scharr lead to similar IQA results. The Prewitt filters along horizontal (x) and vertical (y) directions are defined as:

$$\mathbf{h}_x = \begin{bmatrix} 1/3 & 0 & -1/3 \\ 1/3 & 0 & -1/3 \\ 1/3 & 0 & -1/3 \end{bmatrix}, \mathbf{h}_y = \begin{bmatrix} 1/3 & 1/3 & 1/3 \\ 0 & 0 & 0 \\ -1/3 & -1/3 & -1/3 \end{bmatrix} \quad (1)$$

Convolving \mathbf{h}_x and \mathbf{h}_y with the reference and distorted images yields the horizontal and vertical gradient images of \mathbf{r} and \mathbf{d} . The gradient magnitude images of \mathbf{r} and \mathbf{d} are computed as follows:

$$\mathbf{m}_r(i) = \sqrt{(\mathbf{r} \otimes \mathbf{h}_x)^2(i) + (\mathbf{r} \otimes \mathbf{h}_y)^2(i)} \quad (2)$$

$$\mathbf{m}_d(i) = \sqrt{(\mathbf{d} \otimes \mathbf{h}_x)^2(i) + (\mathbf{d} \otimes \mathbf{h}_y)^2(i)} \quad (3)$$

where symbol “ \otimes ” denotes the convolution operation.

With the gradient magnitude images \mathbf{m}_r and \mathbf{m}_d in hand, the gradient magnitude similarity (GMS) map is computed as follows:

$$GMS(i) = \frac{2\mathbf{m}_r(i)\mathbf{m}_d(i) + c}{\mathbf{m}_r^2(i) + \mathbf{m}_d^2(i) + c} \quad (4)$$

where c is a positive constant that supplies numerical stability. (The selection of c will be discussed in Section III-B.) The GMS map is computed in a pixel-wise manner; nonetheless, please note that a value $\mathbf{m}_r(i)$ or $\mathbf{m}_d(i)$ in the gradient magnitude image is computed by a small local patch in the original image \mathbf{r} or \mathbf{d} .

The GMS map serves as the local quality map (LQM) of the distorted image \mathbf{d} . Clearly, if $\mathbf{m}_r(i)$ and $\mathbf{m}_d(i)$ are the same, $GMS(i)$ will achieve the maximal value 1. Let’s use some examples to analyze the GMS induced LQM. The most commonly encountered distortions in many real image processing systems are JPEG compression, JPEG2000 compression, additive white noise (AWN) and Gaussian blur (GB). Referring to Fig. 2, for each of the four types of distortions, two reference images with different contents and their corresponding distorted images are shown (the images are selected from the LIVE database [11]), as well as their gradient magnitude images (\mathbf{m}_r and \mathbf{m}_d) and the corresponding GMS maps. In the GMS map, the brighter the gray level, the higher the similarity, and thus the higher the predicted local quality. These images contain a variety of important structures such as large scale edges, smooth areas and fine textures, etc. A good IQA model should be adaptable to the broad array of possible natural scenes and local structures.

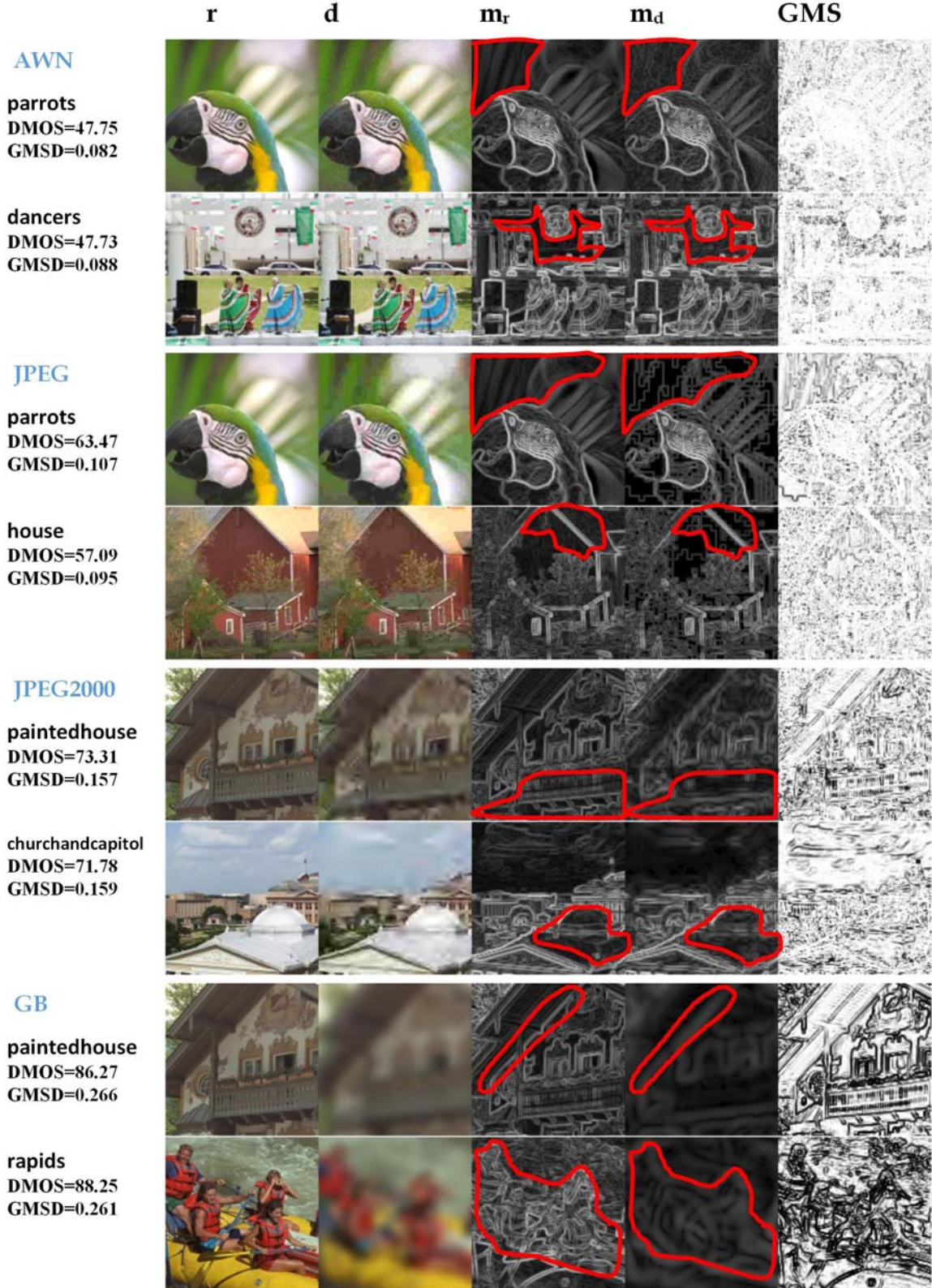


Figure 2: Examples of reference (**r**) and distorted (**d**) images, their gradient magnitude images (**m_r** and **m_d**), and the associated gradient magnitude similarity (GMS) maps, where brighter gray level means higher similarity. The highlighted regions (by red curve) are with clear structural degradation in the gradient magnitude domain. From top to bottom, the four types of distortions are additive white noise (AWN), JPEG compression, JPEG2000 compression, and Gaussian blur (GB). For each type of distortion, two images with different contents are selected from the LIVE database [11]. For each distorted image, its subjective quality score (DMOS) and GMSD index are listed. Note that distorted images with similar DMOS scores have similar GMSD indices, though their contents are totally different.

In Fig. 2, examples of structure degradation are shown in the gradient magnitude domain and marked with red curves. From the first group, it can be seen that the artifacts caused by AWN are masked in the large structure and texture areas, while the artifacts are more visible in flat areas, broadly consistent with perception. In the second group, the artifacts caused by JPEG compression are mainly blocking effects in the background of the image *parrots* and on the wall of image *house*, and loss of fine detail in some places. Clearly, the GMS map is highly responsive to these distortions. Regarding JPEG2000 compression and GB, artifacts are both introduced in the vicinity of edge structures and textured areas. The corresponding GMS maps indicate low quality in these areas. All of these observations imply that the image gradient magnitude is a highly relevant feature for the task of IQA.

B. Pooling with Standard Deviation

The GMS map reflects the local quality of each small patch in the distorted image. The image overall quality score can then be estimated from the GMS based LQM by a pooling stage. The most commonly used pooling strategy is average pooling, i.e., simply averaging the LQM elements as the final IQA score. We refer to the IQA model by applying average pooling to the GMS map as Gradient Magnitude Similarity Mean (GMSM):

$$GMSM = \frac{1}{N} \sum_{i=1}^N GMS(i) \quad (5)$$

where N is the total number of pixels in the image. Clearly, a higher GMSM score means a higher overall image quality. Average pooling assumes that each pixel has the same perceptual quality importance. As introduced in Section I, much effort has been devoted to designing weighted pooling strategies [9, 10, 16, 19, 20 and 29]; however, the improvement brought by weighted pooling over average pooling is not always significant [31] and the computation of weights can be costly.

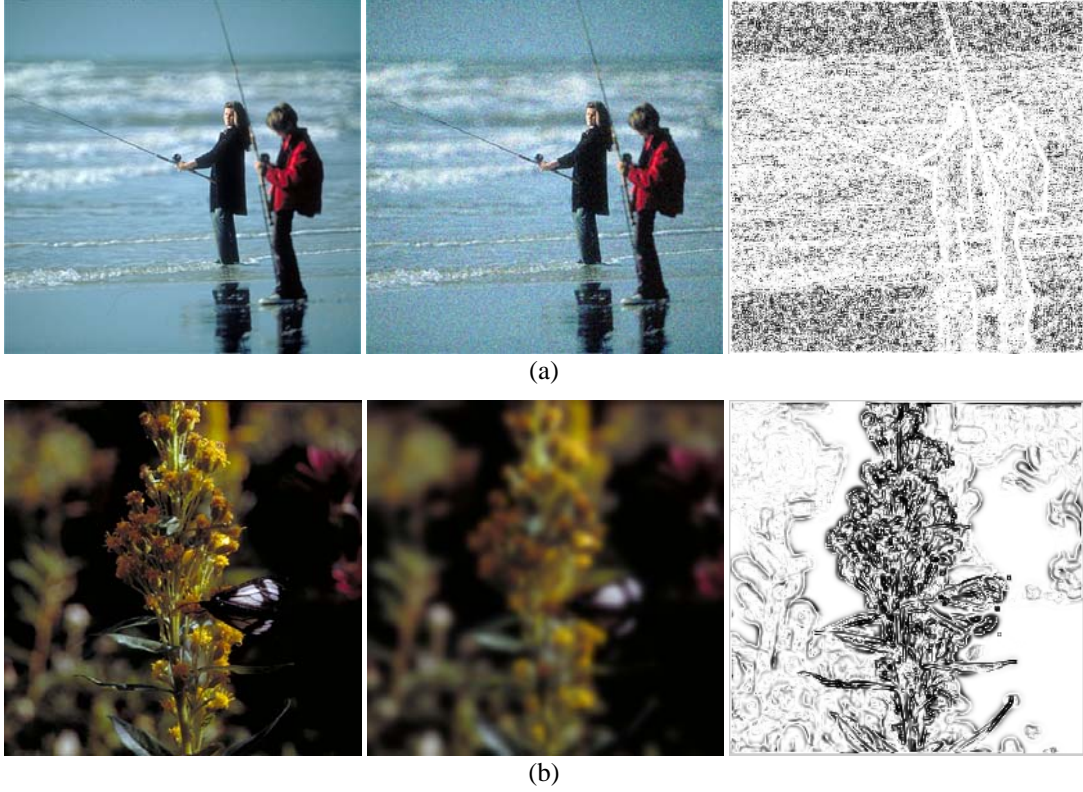


Figure 3: Comparison between GSM and GMSD as a subjective quality indicator. Note that like DMOS, GMSD is a distortion index (a lower DMOS/GMSD means higher quality), while GSM is a quality index (a higher GSM means higher quality). (a) Original image *Fishing*, its Gaussian noise contaminated version (DMOS=0.4403; GSM=0.8853; GMSD=0.1420) and their gradient similarity map. (b) Original image *Flower*, its blurred version (DMOS=0.7785; GSM=0.8745; GMSD=0.1946) and their gradient similarity map. Based on the human subjective DMOS, image *Fishing* has higher quality than image *Flower*. GMSD gives the correct judgement but GSM fails.

We propose a new pooling strategy for the GSM map. A natural image generally has many different types of local structure in its scene. When an image is distorted, the different structures in it will suffer different degradations in gradient magnitude. This is an inherent property of natural images. For example, the distortions introduced by JPEG2000 compression include blocking, ringing, blurring, etc. Blurring will cause less quality degradation in flat areas than in textured areas, while blocking will cause higher quality degradation in flat areas than in textured areas. However, the mean pooling strategy ignores this property and it cannot reflect how the local quality degradation varies. Based on the idea that the global variation of image local quality degradation may reflect its overall quality, we compute the standard deviation of the GSM map and take it as the IQA index, called Gradient Magnitude Similarity Deviation (GMSD):

$$GMSD = \sqrt{\frac{1}{N} \sum_{i=1}^N (GMS(i) - GMSM)^2} \quad (6)$$

Note that the value of GMSD reflects the range of distortion severities in an image. The higher the GMSD

score, the larger the distortion range, and thus the lower the image perceptual quality.

In Fig. 3, we show two original images from the CSIQ database [12], their distorted images and the corresponding GMS maps. The first image *Fishing* is corrupted by additive white noise, and the second image *Flower* is Gaussian blurred. From the GMS map of distorted image *Fishing*, we can see that its local quality is more homogenous, while from the GMS map of distorted image *Flower*, we can clearly see that its local quality in the center area is much worse than at other areas. The human subjective DMOS scores of the two images are 0.4403 and 0.7785, respectively, indicating that the quality of the first image is better than the second one. (Note that like GMSD, DMOS also measures distortion; the lower it is, the better the image quality.) By using GSM, however, the predicted quality scores of the two images are 0.8853 and 0.8745, respectively, indicating that the perceptual quality of the first image is worse than the second one, which is in contradiction to the subjective DMOS scores.

By using GMSD, the predicted quality scores of the two images are 0.1420 and 0.1946, respectively, which is a consistent judgment relative to the subjective DMOS scores, i.e., the first distorted image has better quality than the second one. More examples of the consistency between GMSD and DMOS can be found in Fig. 2. From each distortion type, the two images of different contents have similar DMOS scores, while their GMSD indices are also very close. These examples validate that the deviation pooling strategy coupled with the GMS quality map can accurately predict the perceptual image quality.

III. EXPERIMENTAL RESULTS AND ANALYSIS

A. Databases and Evaluation Protocols

The performance of an IQA model is typically evaluated from three aspects regarding its prediction power: prediction *accuracy*, prediction *monotonicity*, and prediction *consistency* [21]. The computation of the Pearson correlation coefficient to measure the (linear) prediction accuracy requires a curve-fitting procedure [21]. We denote by Q , Q_p and S the original IQA score, the IQA score after regression and the subjective score, respectively. The logistic regression function is defined as:

$$Q_p = \beta_1 \left(\frac{1}{2} - \frac{1}{\exp(\beta_2(Q - \beta_3))} \right) + \beta_4 Q + \beta_5 \quad (7)$$

where $\beta_1, \beta_2, \beta_3, \beta_4$ and β_5 are regression model parameters. After the regression, 3 correspondence indices can be computed for performance evaluation: 1) the Pearson linear correlation coefficient (PCC) between Q_p and S for evaluating the prediction accuracy; 2) the Spearman rank order correlation coefficient (SRC) between Q and S for evaluating the prediction monotonicity; and 3) the RMSE between Q_p and S for evaluating the prediction consistency. Note that the logistic regression does not affect the SRC index. Hence we compute the SRC before regression, that is, between Q and S .

We test the IQA models by employing three large scale publicly accessible IQA databases: LIVE [11], CSIQ [12], and TID2008 [13]. The LIVE database consists of 779 distorted images generated from 29 original images. 5 types of distortions are applied to the reference images at various levels: JPEG2000 compression, JPEG compression, additive white noise (AWN), Gaussian blur (GB) and simulated fast fading Rayleigh channel (FF). These distortions reflect a broad range of image impairments, for example, edge smoothing, block artifacts and random noise. The CSIQ database is composed of 30 original images and their distorted counterparts with six types of distortions at five different distortion levels: JPEG2000, JPEG, AWN, GB, global contrast decrements (CTD), and additive pink Gaussian noise (PGN). There are a total of 886 distorted images in it. The TID2008 database is the largest IQA database to date. It has 1700 distorted images, generated from 25 reference images with 17 types of distortions at 4 levels. Refer to [13] for details of the distortions. Each of the images in these databases has been evaluated by human subjects under controlled conditions, and then assigned a subjective quality score – Mean Opinion Score (MOS) or Difference MOS (DMOS) – to quantize the subjective quality of the image.

To demonstrate the performance of GMSD, we compare it with 11 state-of-the-art and representative FR-IQA models, including PSNR, IFC [22], VIF [23], SSIM [8], MS-SSIM [17], MAD [12], FSIM [7], IW-SSIM [16], G-SSIM [6], GSD [5], and GS [15]. Among them, FSIM, G-SSIM, GSD and GS exploit gradient information. Except for G-SSIM and GSD, which are implemented by us, the source codes of all the other models were obtained from the original authors. To more clearly demonstrate the effectiveness of the proposed deviation pooling strategy, we also present the results of GSM, which uses average pooling. As in most of the previous literature [7-8, 16-17], all of the competing algorithms are applied to the luminance channel of the test images.

B. Implementation of GMSD

The only parameter in the proposed GSM and GMSD models is the constant c in Eq. (4). Apart from ensuring numerical stability, this constant also plays a role in mediating the contrast response in low gradient areas. Fig. 4 plots the SRC curves against c by applying GMSD to the LIVE, CSIQ and TID2008 databases. One can see that when c is greater than 100, the SRC curves become flat on all the databases. In our implementation, we set $c=170$. The value of c is proportional to the gray level of images. We can re-write c as $c=(255 \cdot k)^2$ for 8-bit grayscale images. Then $c=170$ corresponds to $k=0.05$. In addition, as in the publicly available implementations of SSIM [8] and FSIM [7], the images \mathbf{r} and \mathbf{d} are first filtered by a 2×2 average filter, and then down-sampled by a factor of 2. Matlab source code that implements GMSD method can be downloaded at <http://www4.comp.polyu.edu.hk/~cslzhang/IQA/GMSD/GMSD.htm>.

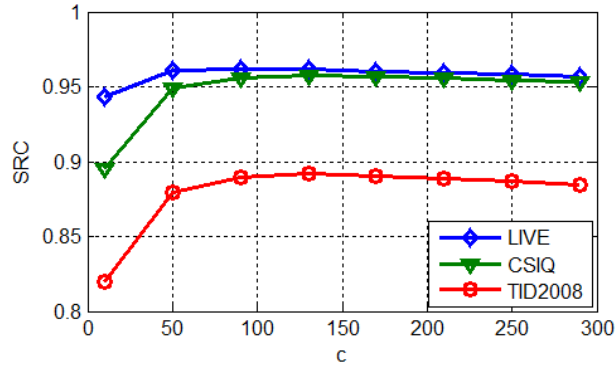


Figure 4: The performance of GMSD in terms of SRC vs. constant c on the three databases.

C. Performance Comparison

In Table I, we compare the competing IQA models' performance on each of the three IQA databases in terms of SRC, PCC and RMSE. The top three models for each evaluation criterion are shown in boldface. We can see that the top models are mostly GMSD (9 times), FSIM (7 times), IW-SSIM (6 times) and VIF (5 times). In terms of all the three criteria (SRC, PCC and RMSE), the proposed GMSD outperforms all the other models on the TID2008 and CSIQ databases. On the LIVE database, VIF, FSIM and GMSD perform almost the same. Compared with gradient based models such as GSD, G-SSIM and GS, GMSD outperforms by a large margin. Compared with GSM, the superiority of GMSD is obvious, showing that the proposed deviation pooling

strategy works much better than the average pooling strategy on the GMS induced LQM. The FSIM algorithm also employs gradient similarity. It performs similarly to GMSD on the LIVE and TID2008 databases, but lags GMSD on the CSIQ database with a lower SRC/PCC and larger RMSE.

Table I: Performance of the proposed GMSD and the other eleven competing FR-IQA models in terms of SRC, PCC, and RMSE on the 3 databases. The top three models for each criterion are shown in boldface.

| <i>IQA model</i> | LIVE (779 images) | | | CSIQ (886 images) | | | TID2008 (1700 images) | | | Weighted Average | |
|---------------------|-------------------|--------------|-------------|-------------------|--------------|--------------|-----------------------|--------------|--------------|------------------|--------------|
| | SRC | PCC | RMSE | SRC | PCC | RMSE | SRC | PCC | RMSE | SRC | PCC |
| <i>PSNR</i> | 0.876 | 0.872 | 13.36 | 0.806 | 0.751 | 0.173 | 0.553 | 0.523 | 1.144 | 0.694 | 0.664 |
| <i>IFC</i> [22] | 0.926 | 0.927 | 10.26 | 0.767 | 0.837 | 0.144 | 0.568 | 0.203 | 1.314 | 0.703 | 0.537 |
| <i>GSD</i> [5] | 0.908 | 0.913 | 11.149 | 0.854 | 0.854 | 0.137 | 0.657 | 0.707 | 0.949 | 0.766 | 0.793 |
| <i>G-SSIM</i> [6] | 0.918 | 0.920 | 10.74 | 0.872 | 0.874 | 0.127 | 0.731 | 0.760 | 0.873 | 0.811 | 0.827 |
| <i>SSIM</i> [8] | 0.948 | 0.945 | 8.95 | 0.876 | 0.861 | 0.133 | 0.775 | 0.773 | 0.851 | 0.841 | 0.836 |
| <i>VIF</i> [23] | 0.964 | 0.960 | 7.61 | 0.919 | 0.928 | 0.098 | 0.749 | 0.808 | 0.790 | 0.844 | 0.875 |
| <i>MAD</i> [12] | 0.944 | 0.939 | 9.37 | 0.899 | 0.820 | 0.150 | 0.771 | 0.748 | 0.891 | 0.845 | 0.811 |
| <i>MS-SSIM</i> [17] | 0.952 | 0.950 | 8.56 | 0.877 | 0.659 | 0.197 | 0.809 | 0.801 | 0.803 | 0.860 | 0.798 |
| <i>GS</i> [15] | 0.956 | 0.951 | 8.43 | 0.911 | 0.896 | 0.116 | 0.850 | 0.842 | 0.723 | 0.891 | 0.882 |
| <i>GMSM</i> | 0.960 | 0.956 | 8.049 | 0.929 | 0.913 | 0.107 | 0.848 | 0.837 | 0.735 | 0.895 | 0.884 |
| <i>IW-SSIM</i> [16] | 0.957 | 0.952 | 8.35 | 0.921 | 0.914 | 0.106 | 0.856 | 0.858 | 0.689 | 0.896 | 0.895 |
| <i>FSIM</i> [7] | 0.963 | 0.960 | 7.67 | 0.924 | 0.912 | 0.108 | 0.880 | 0.874 | 0.653 | 0.911 | 0.904 |
| <i>GMSD</i> | 0.960 | 0.960 | 7.62 | 0.957 | 0.954 | 0.079 | 0.891 | 0.879 | 0.640 | 0.924 | 0.917 |

Table II: Ranking of GMSD, GMSM and the other eleven competing FR-IQA models in terms of SRC.

| <i>IQA metric</i> | LIVE | CSIQ | TID2008 | Weighted Average |
|---------------------|------|------|---------|------------------|
| <i>PSNR</i> | 13 | 12 | 13 | 13 |
| <i>IFC</i> [22] | 10 | 13 | 12 | 12 |
| <i>GSD</i> [5] | 12 | 11 | 11 | 11 |
| <i>G-SSIM</i> [6] | 11 | 10 | 10 | 10 |
| <i>SSIM</i> [8] | 8 | 9 | 7 | 9 |
| <i>VIF</i> [23] | 1 | 5 | 9 | 8 |
| <i>MAD</i> [12] | 9 | 7 | 8 | 7 |
| <i>MS-SSIM</i> [17] | 7 | 8 | 6 | 6 |
| <i>GS</i> [15] | 6 | 6 | 4 | 5 |
| <i>GMSM</i> | 4 | 2 | 5 | 4 |
| <i>IW-SSIM</i> [16] | 5 | 4 | 3 | 3 |
| <i>FSIM</i> [7] | 2 | 3 | 2 | 2 |
| <i>GMSD</i> | 3 | 1 | 1 | 1 |

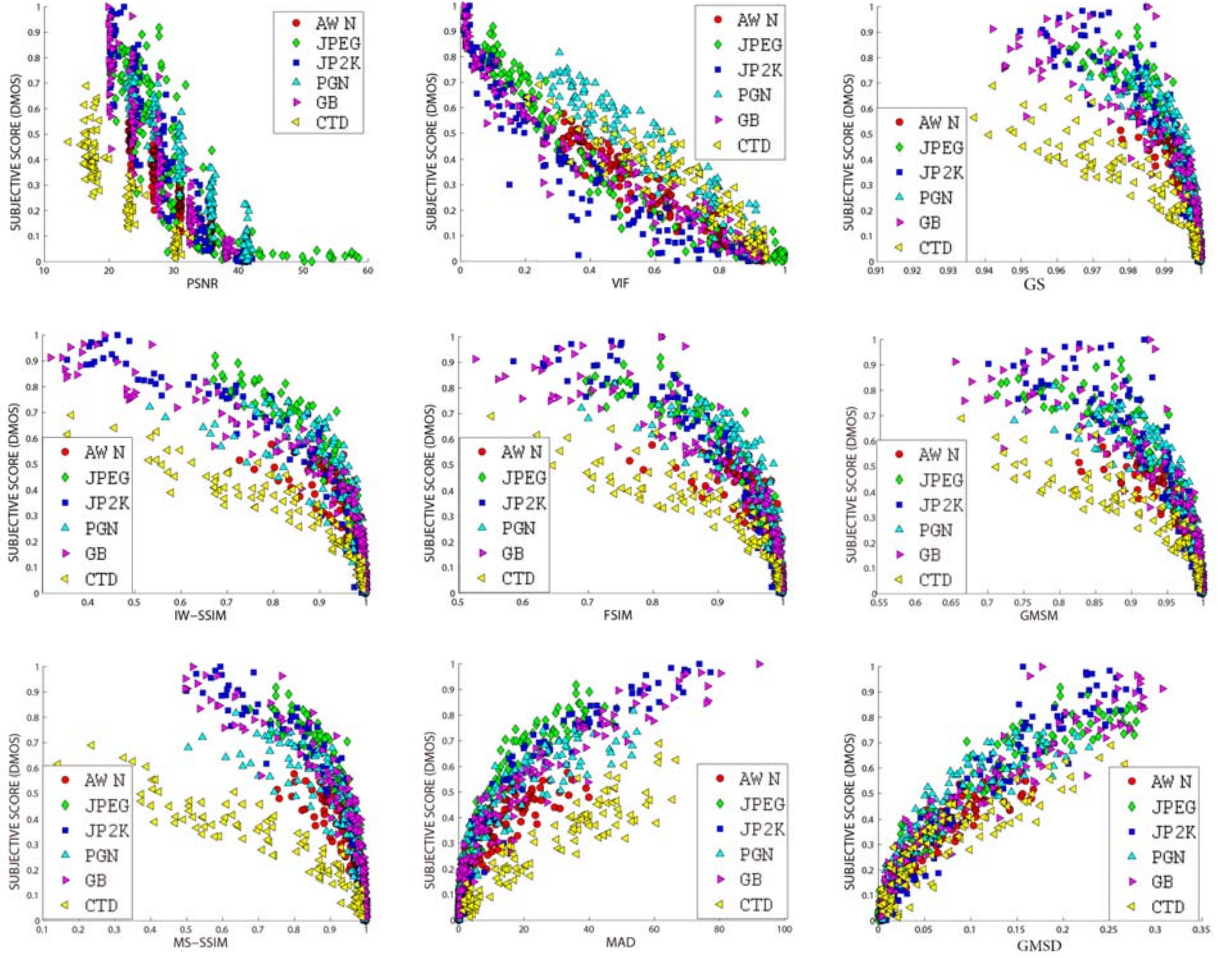


Figure 5: Scatter plots of predicted quality scores against the subjective quality scores (DMOS) by representative FR-IQA models on the CSIQ database. The six types of distortions are represented by different shaped colors.

In Fig. 5, we show scatter plots of predicted quality scores against subjective quality scores (i.e., DMOS scores) for some representative models (PSNR, VIF, GS, IW-SSIM, MS-SSIM, MAD, FSIM, GSM and GMSD) on the CSIQ database, which has six types of distortions (AWN, JPEG, JPEG2000, PGN, GB and CTD). One can observe that for FSIM, MAD, MS-SSIM, GSM, IW-SSIM and GS, the performance distributions on the CTD distortion deviates much from the performance distributions on other types of distortions, degrading their overall performances. When the distortion is severe (large DMOS value), GS, GSM, and PSNR yield less accurate quality predictions. The information fidelity based VIF performs very well on the LIVE database, but not so well on the other two databases. This is mainly because VIF does not predict consistently the images' quality across different distortion types on these two databases, as can be observed from the scatter plots in Fig. 5.

| LIVE | PSNR | IFC | GSD | G-SSIM | SSIM | VIF | MAD | MS-SSIM | GS | GMSM | IW-SSIM | FSIM | GMSD |
|---------|------|-----|-----|--------|------|-----|-----|---------|----|------|---------|------|------|
| PSNR | 0 | 0 | 0 | 0 | 0 | 0 | 0 | 0 | 0 | 0 | 0 | 0 | 0 |
| IFC | 1 | 0 | 1 | 0 | 0 | 0 | 0 | 0 | 0 | 0 | 0 | 0 | 0 |
| GSD | 1 | 0 | 0 | 0 | 0 | 0 | 0 | 0 | 0 | 0 | 0 | 0 | 0 |
| G-SSIM | 1 | 0 | 0 | 0 | 0 | 0 | 0 | 0 | 0 | 0 | 0 | 0 | 0 |
| SSIM | 1 | 1 | 1 | 1 | 0 | 0 | 0 | 0 | 0 | 0 | 0 | 0 | 0 |
| VIF | 1 | 1 | 1 | 1 | 1 | 0 | 1 | 1 | 1 | 0 | 1 | 0 | 0 |
| MAD | 1 | 1 | 1 | 1 | 0 | 0 | 0 | 0 | 0 | 0 | 0 | 0 | 0 |
| MS-SSIM | 1 | 1 | 1 | 1 | 0 | 0 | 1 | 0 | 0 | 0 | 0 | 0 | 0 |
| GS | 1 | 1 | 1 | 1 | 1 | 0 | 1 | 0 | 0 | 0 | 0 | 0 | 0 |
| GMSM | 1 | 1 | 1 | 1 | 1 | 0 | 1 | 1 | 0 | 0 | 0 | 0 | 0 |
| IW-SSIM | 1 | 1 | 1 | 1 | 1 | 0 | 1 | 0 | 0 | 0 | 0 | 0 | 0 |
| FSIM | 1 | 1 | 1 | 1 | 1 | 0 | 1 | 1 | 1 | 0 | 1 | 0 | 0 |
| GMSD | 1 | 1 | 1 | 1 | 1 | 0 | 1 | 1 | 1 | 0 | 1 | 0 | 0 |

(a)

| CSIQ | PSNR | IFC | GSD | G-SSIM | SSIM | VIF | MAD | MS-SSIM | GS | GMSM | IW-SSIM | FSIM | GMSD |
|---------|------|-----|-----|--------|------|-----|-----|---------|----|------|---------|------|------|
| PSNR | 0 | 0 | 0 | 0 | 0 | 0 | 0 | 1 | 0 | 0 | 0 | 0 | 0 |
| IFC | 1 | 0 | 0 | 0 | 0 | 0 | 0 | 1 | 0 | 0 | 0 | 0 | 0 |
| GSD | 1 | 0 | 0 | 0 | 0 | 0 | 1 | 1 | 0 | 0 | 0 | 0 | 0 |
| G-SSIM | 1 | 1 | 1 | 0 | 0 | 0 | 1 | 1 | 0 | 0 | 0 | 0 | 0 |
| SSIM | 1 | 1 | 0 | 0 | 0 | 0 | 1 | 1 | 0 | 0 | 0 | 0 | 0 |
| VIF | 1 | 1 | 1 | 1 | 1 | 0 | 1 | 1 | 1 | 1 | 1 | 1 | 0 |
| MAD | 1 | 0 | 0 | 0 | 0 | 0 | 0 | 1 | 0 | 0 | 0 | 0 | 0 |
| MS-SSIM | 0 | 0 | 0 | 0 | 0 | 0 | 0 | 0 | 0 | 0 | 0 | 0 | 0 |
| GS | 1 | 1 | 1 | 1 | 1 | 0 | 1 | 1 | 0 | 0 | 0 | 0 | 0 |
| GMSM | 1 | 1 | 1 | 1 | 1 | 0 | 1 | 1 | 1 | 0 | 0 | 0 | 0 |
| IW-SSIM | 1 | 1 | 1 | 1 | 1 | 0 | 1 | 1 | 1 | 0 | 0 | 0 | 0 |
| FSIM | 1 | 1 | 1 | 1 | 1 | 0 | 1 | 1 | 1 | 0 | 0 | 0 | 0 |
| GMSD | 1 | 1 | 1 | 1 | 1 | 1 | 1 | 1 | 1 | 1 | 1 | 1 | 0 |

(b)

| TID2008 | PSNR | IFC | GSD | G-SSIM | SSIM | VIF | MAD | MS-SSIM | GS | GMSM | IW-SSIM | FSIM | GMSD |
|---------|------|-----|-----|--------|------|-----|-----|---------|----|------|---------|------|------|
| PSNR | 0 | 1 | 0 | 0 | 0 | 0 | 0 | 0 | 0 | 0 | 0 | 0 | 0 |
| IFC | 0 | 0 | 0 | 0 | 0 | 0 | 0 | 0 | 0 | 0 | 0 | 0 | 0 |
| GSD | 1 | 1 | 0 | 0 | 0 | 0 | 0 | 0 | 0 | 0 | 0 | 0 | 0 |
| G-SSIM | 1 | 1 | 1 | 0 | 0 | 0 | 0 | 0 | 0 | 0 | 0 | 0 | 0 |
| SSIM | 1 | 1 | 1 | 1 | 0 | 0 | 1 | 0 | 0 | 0 | 0 | 0 | 0 |
| VIF | 1 | 1 | 1 | 1 | 1 | 0 | 1 | 0 | 0 | 0 | 0 | 0 | 0 |
| MAD | 1 | 1 | 1 | 0 | 0 | 0 | 0 | 0 | 0 | 0 | 0 | 0 | 0 |
| MS-SSIM | 1 | 1 | 1 | 1 | 1 | 0 | 1 | 0 | 0 | 0 | 0 | 0 | 0 |
| GS | 1 | 1 | 1 | 1 | 1 | 1 | 1 | 1 | 0 | 0 | 0 | 0 | 0 |
| GMSM | 1 | 1 | 1 | 1 | 1 | 1 | 1 | 1 | 0 | 0 | 0 | 0 | 0 |
| IW-SSIM | 1 | 1 | 1 | 1 | 1 | 1 | 1 | 1 | 1 | 1 | 0 | 0 | 0 |
| FSIM | 1 | 1 | 1 | 1 | 1 | 1 | 1 | 1 | 1 | 1 | 1 | 0 | 0 |
| GMSD | 1 | 1 | 1 | 1 | 1 | 1 | 1 | 1 | 1 | 1 | 1 | 1 | 0 |

(c)

Figure 6: The results of statistical significance tests of the competing IQA models on the (a) LIVE, (b) CSIQ and (c) TID2008 databases. A value of ‘1’ (highlighted in green) indicates that the model in the row is significantly better than the model in the column, while a value of ‘0’ (highlighted in red) indicates that the first model is not significantly better than the second one. Note that the proposed GMSD is significantly better than most of the competitors on all the three databases, while no IQA model is significantly better than GMSD.

In Table I, we also show the weighted average SRC and PCC scores of the competing FR-IQA models over the three databases, where the weights were determined by the size (i.e., number of images) of each database. Table II shows the rankings of the 13 competing IQA models in terms of SRC. The top 3 models are GMSD, FSIM and IW-SSIM. Overall, the proposed GMSD achieves outstanding and consistent performance across the three databases.

In order to make statistically meaningful conclusions on the models’ performance, we further conducted a series of hypothesis tests based on the prediction residuals of each model after nonlinear regression, and show

the results of significance tests in Fig. 6. By assuming that the model's residuals follow a Gaussian distribution (the Jarque-Bera test [35] shows that only 3 models on LIVE and 4 models on CSIQ violate this assumption), we apply the left-tailed F -test to the residuals of every two models to be compared. A value of $H=1$ for the left-tailed F -test at a significance level of 0.05 means that the first model (indicated by the row in Fig. 6) has better IQA performance than the second model (indicated by the column in Fig. 6) with a confidence greater than 95%. A value of $H=0$ means that the first model is not significantly better than the second one. If $H=0$ always holds no matter which one of the two models is taken as the first one, then the models have no significant difference in performance. Figs. 6(a) ~ 6(c) show the significance test results on the LIVE, CSIQ and TID2008 databases, respectively. We see that on the LIVE database, GMSD is significantly better than all the other IQA models except for VIF, GSM and FSIM. On the CSIQ database, GMSD is significantly better than all the other models. On the TID2008 database, GMSD is significantly better than all the other IQA models except for FSIM. Note that on all three databases, no IQA model performs significantly better than GMSD.

D. Performance Comparison on Individual Distortion Types

To more comprehensively evaluate an IQA model's ability to predict image quality degradations caused by specific types of distortions, we compared the performances of competing methods on each type of distortion. The results are listed in Table III. To save space, only the SRC scores are shown. There are a total of 28 groups of distorted images in the three databases. In Table III, we use boldface font to highlight the top 3 models in each group. One can see that GMSD is among the top 3 models 14 times, followed by GS and VIF, which are among the top 3 models 11 and 10 times, respectively. However, neither GS nor VIF ranks among the top 3 in terms of overall performance on the 3 databases. The classical PSNR also performs among the top 3 for 8 groups, and a common point of these 8 groups is that they are all noise contaminated. PSNR is, indeed, an effective measure of perceptual quality of noisy images. However, PSNR is not able to faithfully measure the quality of images impaired by other types of distortions.

Table III: Performance comparison of the IQA models on each individual distortion type in terms of SRC.

| | | <i>PSNR</i> | <i>IFC</i> | <i>GSD</i> | <i>G-SSIM</i> | <i>SSIM</i> | <i>VIF</i> | <i>MAD</i> | <i>MS-SSIM</i> | <i>GS</i> | <i>GMSM</i> | <i>IW-SSIM</i> | <i>FSIM</i> | <i>GMSD</i> |
|-------------------------|--------------|--------------|--------------|--------------|---------------|--------------|--------------|--------------|----------------|--------------|--------------|----------------|--------------|--------------|
| <i>LIVE database</i> | <i>JP2K</i> | 0.895 | 0.911 | 0.911 | 0.935 | 0.961 | 0.970 | 0.964 | 0.963 | 0.970 | 0.968 | 0.965 | 0.971 | 0.971 |
| | <i>JPEG</i> | 0.881 | 0.947 | 0.931 | 0.944 | 0.976 | 0.985 | 0.975 | 0.982 | 0.978 | 0.979 | 0.981 | 0.983 | 0.978 |
| | <i>AWN</i> | 0.985 | 0.938 | 0.879 | 0.926 | 0.969 | 0.986 | 0.986 | 0.977 | 0.977 | 0.967 | 0.967 | 0.965 | 0.974 |
| | <i>GB</i> | 0.782 | 0.958 | 0.964 | 0.968 | 0.952 | 0.973 | 0.933 | 0.955 | 0.952 | 0.959 | 0.972 | 0.971 | 0.957 |
| | <i>FF</i> | 0.891 | 0.963 | 0.953 | 0.948 | 0.956 | 0.965 | 0.956 | 0.941 | 0.940 | 0.943 | 0.944 | 0.950 | 0.942 |
| <i>CSIQ database</i> | <i>AWN</i> | 0.936 | 0.843 | 0.732 | 0.810 | 0.897 | 0.957 | 0.960 | 0.944 | 0.944 | 0.962 | 0.938 | 0.926 | 0.968 |
| | <i>JPEG</i> | 0.888 | 0.941 | 0.927 | 0.927 | 0.954 | 0.970 | 0.967 | 0.964 | 0.963 | 0.959 | 0.966 | 0.966 | 0.965 |
| | <i>JP2K</i> | 0.936 | 0.925 | 0.913 | 0.932 | 0.960 | 0.967 | 0.977 | 0.972 | 0.965 | 0.957 | 0.968 | 0.968 | 0.972 |
| | <i>PGN</i> | 0.934 | 0.826 | 0.731 | 0.796 | 0.892 | 0.951 | 0.954 | 0.933 | 0.939 | 0.945 | 0.906 | 0.923 | 0.950 |
| | <i>GB</i> | 0.929 | 0.953 | 0.960 | 0.958 | 0.961 | 0.974 | 0.966 | 0.975 | 0.959 | 0.958 | 0.978 | 0.972 | 0.971 |
| | <i>CTD</i> | 0.862 | 0.487 | 0.948 | 0.851 | 0.793 | 0.934 | 0.917 | 0.945 | 0.936 | 0.933 | 0.954 | 0.942 | 0.904 |
| <i>TID2008 database</i> | <i>AWN</i> | 0.907 | 0.581 | 0.535 | 0.574 | 0.811 | 0.880 | 0.864 | 0.812 | 0.861 | 0.887 | 0.787 | 0.857 | 0.918 |
| | <i>ANMC</i> | 0.899 | 0.546 | 0.479 | 0.556 | 0.803 | 0.876 | 0.839 | 0.807 | 0.809 | 0.877 | 0.792 | 0.851 | 0.898 |
| | <i>SCN</i> | 0.917 | 0.596 | 0.568 | 0.600 | 0.815 | 0.870 | 0.898 | 0.826 | 0.894 | 0.877 | 0.771 | 0.848 | 0.913 |
| | <i>MN</i> | 0.852 | 0.673 | 0.586 | 0.609 | 0.779 | 0.868 | 0.734 | 0.802 | 0.745 | 0.760 | 0.809 | 0.802 | 0.709 |
| | <i>HFN</i> | 0.927 | 0.732 | 0.661 | 0.728 | 0.873 | 0.907 | 0.896 | 0.871 | 0.895 | 0.915 | 0.866 | 0.909 | 0.919 |
| | <i>IMN</i> | 0.872 | 0.534 | 0.577 | 0.409 | 0.673 | 0.833 | 0.513 | 0.698 | 0.723 | 0.748 | 0.646 | 0.746 | 0.661 |
| | <i>QN</i> | 0.870 | 0.586 | 0.609 | 0.672 | 0.853 | 0.797 | 0.850 | 0.852 | 0.880 | 0.867 | 0.818 | 0.855 | 0.887 |
| | <i>GB</i> | 0.870 | 0.856 | 0.911 | 0.924 | 0.954 | 0.954 | 0.914 | 0.954 | 0.960 | 0.952 | 0.964 | 0.947 | 0.897 |
| | <i>DEN</i> | 0.942 | 0.797 | 0.878 | 0.880 | 0.953 | 0.916 | 0.945 | 0.961 | 0.972 | 0.966 | 0.947 | 0.960 | 0.975 |
| | <i>JPEG</i> | 0.872 | 0.818 | 0.839 | 0.859 | 0.925 | 0.917 | 0.942 | 0.939 | 0.939 | 0.939 | 0.918 | 0.928 | 0.952 |
| | <i>JP2K</i> | 0.813 | 0.944 | 0.923 | 0.944 | 0.962 | 0.971 | 0.972 | 0.970 | 0.976 | 0.973 | 0.974 | 0.977 | 0.980 |
| | <i>JGTE</i> | 0.752 | 0.791 | 0.880 | 0.855 | 0.868 | 0.859 | 0.851 | 0.872 | 0.879 | 0.882 | 0.859 | 0.871 | 0.862 |
| | <i>J2TE</i> | 0.831 | 0.730 | 0.722 | 0.758 | 0.858 | 0.850 | 0.840 | 0.861 | 0.894 | 0.877 | 0.820 | 0.854 | 0.883 |
| | <i>NEPN</i> | 0.581 | 0.842 | 0.770 | 0.754 | 0.711 | 0.762 | 0.837 | 0.752 | 0.739 | 0.744 | 0.772 | 0.749 | 0.760 |
| | <i>Block</i> | 0.619 | 0.677 | 0.811 | 0.810 | 0.846 | 0.832 | 0.159 | 0.499 | 0.886 | 0.899 | 0.762 | 0.849 | 0.897 |
| | <i>MS</i> | 0.696 | 0.425 | 0.441 | 0.715 | 0.723 | 0.510 | 0.587 | 0.773 | 0.719 | 0.630 | 0.707 | 0.669 | 0.649 |
| | <i>CTC</i> | 0.586 | 0.171 | 0.573 | 0.552 | 0.525 | 0.819 | 0.493 | 0.625 | 0.669 | 0.663 | 0.630 | 0.648 | 0.466 |

Generally speaking, performing well on specific types of individual distortions does not guarantee that an IQA model will perform well on a broad spectrum of distortion types. A good model should be monotonic to subjective quality not only within a given group of distortions, but also across different distortions. Referring to the scatter plots in Fig. 5, it can be easily seen that the scatter plot of *GMSD* is more concentrated across the different groups of distortion types. This implies that *GMSD* predicts the quality of images suffering from different distortions with similar sensitivity, which helps to preserve the monotonicity of the prediction results across different distortions. From Fig. 5, it becomes apparent why *VIF* and *GSIM* perform well for many individual distortion types but not as well on entire databases; that is, they behave rather differently on different types of distortions (e.g., *CTD*), which we might call the Perceived Distortion Alignment problem [43].

The gradient based models G-SSIM and GSD do not show good performance on many types of distortions and on entire databases. G-SSIM computes the local variance and covariance of gradient magnitude to gauge contrast and structure similarity. This may not be an effective way to make use of gradient information. GSD combines the orientation differences of gradient, the contrast similarity and the gradient similarity; however, there is intersection between these kinds of information, making GSD less discriminative of image quality. GMSD only uses the gradient magnitude information but achieves highly competitive results against competing methods. This validates the gradient magnitude, coupled with the deviation pooling strategy, as an excellent predictive image quality feature.

E. Linearity

In order to provide a better mapping between the scores predicted by an algorithm and human subjective scores, a logistic regression via Eq. (7) is ordinarily applied to the predicted quality scores before computing the linear correlation coefficient (LCC). The parameters in the regression model are optimized on the database in the sense of least-square error fitting. However, there is no guarantee that the parameters optimized on the database will also work optimally for real applications. It is highly desirable that an IQA model could straightforwardly yield a high LCC between the predicted quality scores and the subjective quality scores without the need for nonlinear regression. The property of linearity can bring the following benefits.

First, the linearity of an IQA model makes it free of the potential problems caused by regression function learning. To learn the regression function, it is necessary to have a sufficient number of comprehensive training samples in hand, which can be difficult to collect. On the other hand, the statistical properties of the test samples can be different from those of the training samples, resulting in bias of the learned regression function and hence inaccurate quality prediction. For example, if the distortion type in a test sample is out of the training dataset, the learned regression function may fail on this test sample.

Second, the linearity of an IQA model makes it more convenient to use in benchmarking image processing algorithms such as image compression. With a linear IQA model, the difference between the model's prediction scores will be equivalent to the difference of human subjective scores. Therefore, a linear IQA

model will not complicate the relationship between quality degradation and bit allocation for perceptual image compression, while a nonlinear IQA model can make the rate-distortion curve complicated.

None of the existing state-of-the-art FR-IQA models has such a linear property. Interestingly, the proposed GMSD model shows a high linearity. The LCC values of the 13 competing FR-IQA models without nonlinear regression are shown in Table IV. GMSD yields the highest LCC against the subjective scores, outperforming the other models by a significant margin. This can also be observed from the scatter plots in Fig. 5, where the plots of GMSD against DMOS are highly linear and tightly concentrated, implying a strong linearity.

Table IV: LCC of the IQA models without nonlinear regression.

| <i>Models</i> | LIVE | CSIQ | TID2008 | Weighted Average |
|---------------------|--------------|--------------|--------------|------------------|
| <i>IFC [22]</i> | 0.853 | 0.653 | 0.203 | 0.472 |
| <i>PSNR</i> | 0.859 | 0.751 | 0.519 | 0.659 |
| <i>MS-SSIM [17]</i> | 0.759 | 0.659 | 0.757 | 0.732 |
| <i>MAD [12]</i> | 0.763 | 0.820 | 0.714 | 0.753 |
| <i>GS [15]</i> | 0.780 | 0.747 | 0.778 | 0.770 |
| <i>SSIM [8]</i> | 0.829 | 0.792 | 0.740 | 0.774 |
| <i>GSD [5]</i> | 0.906 | 0.844 | 0.698 | 0.785 |
| <i>GMSM</i> | 0.850 | 0.802 | 0.775 | 0.799 |
| <i>IW-SSIM [16]</i> | 0.803 | 0.795 | 0.809 | 0.804 |
| <i>G-SSIM [6]</i> | 0.889 | 0.853 | 0.753 | 0.811 |
| <i>FSIM [7]</i> | 0.859 | 0.805 | 0.830 | 0.830 |
| <i>VIF [23]</i> | 0.941 | 0.922 | 0.777 | 0.853 |
| <i>GMSD</i> | 0.942 | 0.929 | 0.872 | 0.903 |

F. Standard Deviation Pooling on Other IQA Models

As discussed in previous sections, the method of standard deviation (SD) pooling applied to the GMS map leads to significantly elevated performance of image quality prediction. It is therefore natural to wonder whether the SD pooling strategy can deliver similar performance improvement on other IQA models. To explore this, we modified six representative FR-IQA methods, all of which are able to generate an LQM of the test image: MSE (which is equivalent to PSNR but can produce an LQM), SSIM [8], MS-SSIM [17], FSIM [7], G-SSIM [6] and GSD [5]. The original pooling strategies of all of these methods are average pooling or weighted average pooling. In Table V, the SRC results of these methods using both (weighted) average pooling and SD pooling on the LIVE, CSIQ and TID2008 databases are listed.

Table V makes it clear that except for MSE, all the other IQA methods fail to gain in performance using SD pooling instead of their nominal pooling method. The reason may be that in these methods, the LQM is generated using multiple, diverse types of features. The interaction between these features may complicate the estimation of image local quality so that SD pooling does not apply. By contrast, the MSE and GMSD respectively use only the original intensity and the intensity of gradient magnitude, respectively, to calculate the LQM.

Table V: SRC results of SD pooling on some representative IQA models.

| <i>Database</i> | (Weighted) average pooling | | | SD pooling | | | Performance gain | | |
|---------------------|----------------------------|-------|---------|------------|-------|---------|------------------|---------|---------|
| | LIVE | CSIQ | TID2008 | LIVE | CSIQ | TID2008 | LIVE | CSIQ | TID2008 |
| <i>MSE</i> | 0.876 | 0.806 | 0.553 | 0.877 | 0.834 | 0.580 | 0.18% | 3.55% | 4.88% |
| <i>SSIM [8]</i> | 0.948 | 0.876 | 0.775 | 0.917 | 0.817 | 0.756 | -3.22% | -6.71% | -2.44% |
| <i>MS-SSIM [17]</i> | 0.952 | 0.877 | 0.809 | 0.921 | 0.826 | 0.650 | -3.28% | -5.86% | -19.71% |
| <i>FSIM [7]</i> | 0.963 | 0.924 | 0.880 | 0.960 | 0.956 | 0.892 | -0.33% | 3.52% | 1.26% |
| <i>G-SSIM [6]</i> | 0.918 | 0.872 | 0.731 | 0.763 | 0.757 | 0.708 | -16.93% | -13.20% | -3.09% |
| <i>GSD [5]</i> | 0.914 | 0.828 | 0.576 | 0.669 | 0.611 | 0.568 | -26.76% | -26.20% | -1.36% |

G. Complexity

In applications such as real-time image/video quality monitoring and prediction, the complexity of implemented IQA models becomes crucial. We thus analyze the computational complexity of GMSD and compare it with the running time of 13 competing IQA models.

Suppose that an image has N pixels. The classical PSNR has the lowest complexity, and calculating it only requires N multiplications and $2N$ additions. The main operations in the proposed GMSD model include calculation of image gradients (by convolving the image with two 3×3 template integer filters), thereby producing gradient magnitude maps, generating the GMS map and deviation pooling. Overall, it requires $19N$ multiplications and $16N$ additions to yield the final single quality score, and it is only necessary to store at most 4 directional gradient images (each of size N) in memory (at the gradient calculation stage). Therefore, both the time and memory complexities of GMSD are $O(N)$. In other words, the time and memory cost of GMSD scales linearly with the image size, which is a very attractive property since image resolutions have been rapidly increasing with the development of digital imaging technologies. In addition, the computation of image gradients and the GMS map can be parallelized by partitioning the reference and distorted images into blocks if the image size is very large.

Table VI shows the running time of the 13 IQA models on an image of size 512×512 . All algorithms were run on a ThinkPad T420S notebook with Intel Core i7-2600M CPU@2.7GHz and 4G RAM. The software platform for all algorithms was MATLAB R2010a (7.10). Apart from G-SSIM and GSD, the Matlab source codes of all the other methods were obtained from the original authors. (It should be noted that whether the code is optimized may affect the running time of an algorithm.) Clearly, PSNR is the fastest, followed by GSM and GMSD. Specifically, it costs only 0.0110 second for GMSD to process an image of size 512×512 , which is 3.5 times faster than SSIM, 47.9 times faster than FSIM, and 106.7 times faster than VIF.

Table VI: Running time of the competing IQA models.

| <i>Models</i> | <i>Running time (s)</i> |
|---------------------|-------------------------|
| <i>MAD [12]</i> | 28.996 |
| <i>IFC [22]</i> | 1.1811 |
| <i>VIF [23]</i> | 1.1745 |
| <i>FSIM [7]</i> | 0.5269 |
| <i>IW-SSIM [16]</i> | 0.5196 |
| <i>MS-SSIM [17]</i> | 0.1379 |
| <i>GS [15]</i> | 0.0899 |
| <i>GSD [5]</i> | 0.0481 |
| <i>SSIM [8]</i> | 0.0388 |
| <i>G-SSIM [6]</i> | 0.0379 |
| <i>GMSD</i> | 0.0110 |
| <i>GSM</i> | 0.0079 |
| <i>PSNR</i> | 0.0016 |

H. Discussions

Apart from being used purely for quality assessment tasks, it is expected that IQA algorithms can be more pervasively used in many others applications. According to [1], the most common applications of IQA algorithms can be categorized as follows: 1) quality monitoring; 2) performance evaluation; 3) system optimization; and 4) perceptual fidelity criteria on visual signals. Quality monitoring is usually conducted by using no reference IQA models, while FR-IQA models can be applied to the other three categories. Certainly, SSIM proved to be a milestone in the development of FR-IQA models. It has been widely and successfully used in the performance evaluation of many image processing systems and algorithms, such as image compression, restoration, half-toning, fusion and communication, etc. (The code of SSIM is freely available at [39].) Apart from performance evaluation, thus far, SSIM is not yet pervasively used in other applications. The reason may be two-fold, as discussed below. The proposed GMSD model might alleviate these problems

associated with SSIM, yielding the potentials to be more pervasively used in a wider variety of image processing applications.

First, SSIM is difficult to optimize when it is used as a fidelity criterion on visual signals. This largely restricts its applications in designing image processing algorithms such as image compression, restoration, half-toning and fusion, etc. Recently, some works [36-38] have been reported to adopt SSIM for image/video perceptual compression. However, the proposed methods are generally not “one-pass” and have high complexity. Compared with SSIM, the formulation of GMSD is much simpler. Only the calculation of gradient magnitude maps and their correlation is involved. GMSD may be more easily optimized than SSIM, hence it has great potential to be used as a fidelity criterion for designing perceptual image compression and restoration algorithms, as well as for perceptually optimizing network coding and resource allocation problems.

Second, the time and memory complexity of SSIM is relatively high, restricting its use in applications where low-cost and real-time implementation is required, although faster implementations of SSIM have been proposed [42]. GMSD is much faster and more scalable than SSIM, and thus it can be easily adopted for tasks such as real time performance evaluation, system optimization, etc. Considering that mobile and portable devices are becoming much more popular, the merits of simplicity, low complexity and high accuracy of GMSD make it very attractive and competitive for mobile applications.

In addition, it should be noted that with the rapid development of digital image acquisition and display technologies, and the increasing popularity of mobile devices and websites such as YouTube and Facebook, current IQA databases may not fully represent the way that human subjects view digital images. On the other hand, the current databases, including the three largest ones TID2008, LIVE and CSIQ, mainly focus on a few classical distortion types, and the images therein undergo only a single type of distortion. Therefore, there is a demand to establish new IQA databases, which should contain images with multiple types of distortions [40], images collected from mobile devices [41], and images of high definition.

IV. CONCLUSION

The usefulness and effectiveness of the image gradient for full reference image quality assessment (FR-IQA)

were studied in this paper. We devised a simple FR-IQA model called gradient magnitude similarity deviation (GMSD), where the pixel-wise gradient magnitude similarity (GMS) is used to capture image local quality, and the standard deviation of the overall GMS map is used as the pooling strategy for the final image quality index. Such a standard deviation based pooling strategy is based on the consideration that the variation of local quality, which arises from the diversity of image local structures, is highly relevant to subjective image quality. Compared with state-of-the-art FR-IQA models, the proposed GMSD model performs the best in terms of both accuracy and efficiency. Furthermore, GMSD exhibits high linearity w.r.t. subjective quality scores even without nonlinear regression. All of these properties make GMSD an ideal choice for practical real-time and high performance IQA applications.

REFERENCES

- [1] Z. Wang, "Applications of objective image quality assessment methods," *IEEE Signal Processing Magazine*, vol. 28, no. 6, pp. 137–142, Nov. 2011.
- [2] B. Girod, "What's wrong with mean-squared error?" *Digital Images and Human Vision*. MIT press, 1993.
- [3] Z. Wang, and A. C. Bovik, "Modern Image Quality Assessment," *Synthesis Lectures on Image, Video, and Multimedia Processing*, vol. 2, no.1, pp. 1-156, 2006.
- [4] D. O. Kim, H. S. Han, and R. H. Park, "Gradient information-based image quality metric," *IEEE Transactions on Consumer Electronics*, vol. 56, no. 2, pp. 930-936, 2010.
- [5] G. Q. Cheng, J. C. Huang, C. Zhu, Z. Liu and L. Z. Cheng, "Perceptual image quality assessment using a geometric structural distortion model," 17th *IEEE International Conference on Image Processing*, 2010.
- [6] G. H. Chen, C. L. Yang and S. L. Xie, "Gradient-based structural similarity for image quality assessment," 13th *IEEE International Conference on Image Processing*, 2006.
- [7] Lin Zhang, Lei Zhang, X. Mou and D. Zhang, "FSIM: A Feature Similarity Index for Image Quality Assessment," *IEEE Trans. Image Process.*, vol. 20, no. 8, pp. 2378-2386, Aug. 2011.
- [8] Z. Wang, A. C. Bovik and H. R. Sheikh, and E. P. Simoncelli, "Image quality assessment: from error visibility to structural similarity," *IEEE Trans. Image Process.*, vol. 13, no. 4, pp. 600-612, 2004.
- [9] Z. Wang and X. Shang, "Spatial pooling strategies for perceptual image quality assessment," *IEEE Int. Conf. Image Process.*, Sep. 2006, pp. 2945–2948.

- [10] A.K. Moorthy and A.C. Bovik, "Visual importance pooling for image quality assessment," *IEEE J. Special Topics Signal Process*, vol. 3, pp. 193-201, April 2009.
- [11] H. R. Sheikh, Z. Wang, L. Cormack, and A. C. Bovik. (2005) "Live Image Quality Assessment Database Release 2," [Online]. <http://live.ece.utexas.edu/research/quality>.
- [12] Eric C. Larson and Damon M. Chandler, "Most apparent distortion: full-reference image quality assessment and the role of strategy," *J. Electron. Imaging* 19, 011006, Jan 07, 2010.
- [13] N. Ponomarenko, V. Lukin, A. Zelensky, K. Egiazarian, M. Carli, F. Battisti, "TID2008 - A Database for Evaluation of Full-Reference Visual Quality Assessment Metrics," *Advances of Modern Radio electronics*, Vol. 10, pp. 30-45, 2009.
- [14] Lin Zhang, Lei Zhang, X. Mou and D. Zhang, "A Comprehensive Evaluation of Full Reference Image Quality Assessment Algorithms," *IEEE Int. Conf. Image Process*. 2012.
- [15] A. Liu, W. Lin, and Manish Narwaria, "Image Quality Assessment Based on Gradient Similarity," *IEEE Transactions on Image Processing*, vol. 21, no. 4, pp. 1500-1512, 2012.
- [16] Z. Wang, and Q. Li, "Information content weighting for perceptual image quality assessment," *IEEE Transactions on Image Processing*, vol. 20, no. 5, pp. 1185-1198, 2011.
- [17] Z. Wang, E. P. Simoncelli, and A. C. Bovik, "Multiscale structural similarity for image quality assessment," *Conference Record of the Thirty-Seventh Asilomar Conference on Signals, Systems and Computers*, vol. 2, IEEE, 2003.
- [18] M. Zhang, X. Mou, and L. Zhang, "Non-Shift Edge Based Ratio (NSER): An Image Quality Assessment Metric Based on Early Vision Features," *IEEE Signal Processing Letters*, vol. 18, no .5, pp. 315-318, 2011.
- [19] C. F. Li, and A. C. Bovik, "Content-partitioned structural similarity index for image quality assessment," *Signal Processing: Image Communication*, vol. 25, no. 7, pp. 517-526, 2010.
- [20] Y. Tong, Hubert Konik, F. A. Cheikh and Alain Tremeau, "Full reference image quality assessment based on saliency map analysis," *Journal of Imaging Science*, vol. 54, no. 3, pp. 30503-30503, 2010.
- [21] VQEG, "Final report from the Video Quality Experts Group on the validation of objective models of video quality assessment – Phase II," August 2003, available at <http://www.vqeg.org/>.
- [22] H.R. Sheikh, A.C. Bovik and G. de Veciana, "An information fidelity criterion for image quality assessment using natural scene statistics," *IEEE Transactions on Image Processing*, vol.14, no.12pp. 2117- 2128, Dec. 2005.
- [23] H.R. Sheikh. and A.C. Bovik, "Image information and visual quality," *IEEE Transactions on Image Processing*, vol.15, no.2, pp. 430- 444, Feb. 2006.

- [24] W. Xue, and X. Mou, "An image quality assessment metric based on Non-shift Edge," *18th IEEE International Conference on Image Processing (ICIP)*, 2011.
- [25] Z. Wang and A. C. Bovik, "Mean squared error: love it or leave it? - A new look at signal fidelity measures," *IEEE Signal Processing Magazine*, vol. 26, no. 1, pp. 98-117, Jan. 2009.
- [26] A.L. Neuenschwander, M.M. Crawford, L.A. Magruder, C. A. Weed, R. Cannata, D. Fried, R. Knowlton and R. Heinrichs, "Classification of LADAR data over Haitian urban environments using a lower envelope follower and adaptive gradient operator," *Proc. SPIE 7684, 768408* (2010).
- [27] S. A. Coleman, B. W. Scotney, and S. Suganthan, "Multi-scale edge detection on range and intensity images," *Pattern Recognition*, vol. 44, no. 4, pp. 821-838, 2011.
- [28] Nezhadarya Ehsan, and Rabab K. Ward, "An efficient method for robust gradient estimation of RGB color images," *16th IEEE International Conference on Image Processing (ICIP)*, 2009.
- [29] J. Park, K. Seshadrinathan, S. Lee and A.C. Bovik, "VQpooling: Video quality pooling adaptive to perceptual distortion severity," *IEEE Transactions on Image Processing*, vol. 22, no. 2, pp. 610-620, February 2013.
- [30] W. Lin, C.-C. Jay Kuo, "Perceptual visual quality metrics: A survey," *Journal of Visual Communication and Image Representation*, vol. 22, no. 4, pp. 297-312, May 2011.
- [31] Ninassi, Alexandre, et al., "Does where you gaze on an image affect your perception of quality? Applying visual attention to image quality metric," *IEEE International Conference on Image Processing*, vol. 2, 2007.
- [32] J. Ross and H. D. Speed, "Contrast adaptation and contrast masking in human vision," *Proceedings. Biological Sciences / The Royal Society*, vol. 246, no. 1315, pp. 61-9, Oct. 1991.
- [33] S. J. Daly, "Application of a noise-adaptive contrast sensitivity function to image data compression," *Optical Engineering*, vol. 29, pp. 977-987, 1990.
- [34] Lubin, Jeffrey. "A human vision system model for objective picture quality measurements," *International Broadcasting Conference (IBC)*, January 1997 p. 498 – 503.
- [35] Carlos M. Jarque, Anil K. Bera, "Efficient tests for normality, homoscedasticity and serial independence of regression residuals," *Economics Letters* 6 (3): 255-259, 1980.
- [36] Chao Wang, Xuanqin Mou, Wei Hong, and Lei Zhang, "Block-layer bit allocation for quality constrained video encoding based on constant perceptual quality," *Proceedings of SPIE Vol. 8666, 86660J* (2013).
- [37] Tao-Sheng Ou, Yi-Hsin Huang, and Homer H. Chen, "SSIM-based perceptual rate control for video coding," *IEEE Transactions on Circuits and Systems for Video Technology*, vol. 21, no. 5, pp. 682-691, 2011.

- [38] Shiqi Wang, Abdul Rehman, Z. Wang, Siwei Ma, and Wen Gao, "SSIM-motivated rate-distortion optimization for video coding," *IEEE Transactions on Circuits and Systems for Video Technology*, vol. 22, no. 4 (2012): 516-529.
- [39] Z. Wang, A. C. Bovik and H. R. Sheikh, and E. P. Simoncelli, "The SSIM index for image quality assessment," MATLAB implementation available online from: <http://www.cns.nyu.edu/lcv/ssim/ssim.m>.
- [40] D. Jayaraman, A. Mittal, A. K. Moorthy and A. C. Bovik, "LIVE Multiply Distorted Image Quality Database," online at: http://live.ece.utexas.edu/research/quality/live_multidistortedimage.html.
- [41] A. K. Moorthy, L. K. Choi, A. C. Bovik and G. deVeciana, "Video Quality Assessment on Mobile Devices: Subjective, Behavioral and Objective Studies," *IEEE Journal of Selected Topics in Signal Processing*, vol. 6, no. 6, pp. 652-671, October 2012.
- [42] Ming-Jun Chen, and A. C. Bovik, "Fast structural similarity index algorithm," *Journal of Real-Time Image Processing*, vol. 6, no. 4 (2011): 281-287.
- [43] R. Soundararajan and A. C. Bovik, "RRED indices: Reduced reference entropic differencing for image quality assessment," *IEEE Transactions on Image Processing*, vol. 21, no. 2, pp. 517-526, Feb. 2012.